Preprints of the 20th World Congress
The International Federation of Automatic Control
Toulouse, France, July 9-14, 2017

A bicompartmental dynamic tumor growth model ⋆

Dávid Csercsik [*,**] **Johanna Sápi** [*] **Levente Kovács** [*]

[*] *Research and Innovation Center of Óbuda University, Physiological Controls Group, Óbuda University, Budapest, Hungary (e-mail: sapi.johanna@nik.uni-obuda.hu, kovacs.levente@nik.uni-obuda.hu)*
[**] *Faculty of Information Technology and Bionics, Pázmány Péter Catholic University, Budapest, Hungary (e-mail: csercsik@itk.ppke.hu).*

Abstract: We introduce a simple nonlinear dynamic tumor growth model which distinguishes between a core and a peripherial compartment, and accounts for nutrient and congestion-dependent cell proliferation, necrosis and volume growth. The model synthesis procedure considers that later the model shall be extended with mechanisms describing angiogenesis and will be used in control based optimization of anti-angiogenic treatment procedures.

Keywords: Biomedical systems, Tumor growth modelling, Systems biology, Simulations, Concentrated-parameter models

1. INTRODUCTION

Recently it has been shown by Sápi et al. (2015b) that innovative anti-angiogenic therapies may be more effective for treating tumors, compared to conventional dosage protocols. It is straightforward to ask how to optimize such therapies in the context of personalized medicine, in other words, fitting the therapy on the most available level to the particular case. Model-based control is exactly the framework, which is capable of the integration of preliminary knowledge about the process (via the model) and measured data corresponding to the individual case (originating in this case e.g. from imaging methods, blood tests etc).

If one addresses to approach the model-based optimization and control of drug and radiation based tumor therapies, a solid computational model is needed which is capable of describing the elementary aspects of the phenomena of interest and remains on a tractable level of complexity in the same time.

Control oriented tumor-growth modelling raises some questions, which are not easy to answer. One main feature of a tumor is that it grows without control. Chemical reaction network theory (Gunawardena, 2003), for example, which is widely used in the modelling of intra- and inter-cell signaling and metabolism uses concentration-based methods to describe dynamics in the system in question. Since the volume of the tumor increases with time, the application of this framework is not self-evident. There are however novel concentrated-parameter models of tumor growth and angiogenesis using concentrations as state variables (Yang, 2012). The flaw of such one-compartment models is that they can not distinguish between the tumor periphery and the tumor core, even if the processes which take place in the periphery may be significantly different compared to the core dynamics. Our aim is to create a continuous, concentrated parameter ODE (ordinary differential equation) model, which is capable of describing the various phases of tumor growth (as described by Byrne et al. (2003)), without the application of PDEs (partial differential equations).

Hahnfeldt et al. (1999) described a simple, but very phenomenological model, the validity of which has been already questioned by new biological results (Femke and Griffioen, 2007). Tumor growth models from a control perspective have been recently reviewed by Sápi et al. (2015a).

2. MATERIALS AND METHODS

2.1 Modelling Assumptions

First we define the assumptions we would like to formalize later in the paper.

- We assume spherical tumor geometry composed of a core and of a periphery layer.
- Living tumor cells of the periphery proliferate (cellular mitosis) on a rate which depends on the level of nutrient reaching them, and on the level of their actual concentration.
- Living tumor cells of the core necrotize if the level of nutrient reaching them is too low.
- Separation of time scales: we assume that processes of cellular responses are much faster than growth-related mechanisms.

⋆ This project has received funding from the European Research Council (ERC) under the European Union's Horizon 2020 research and innovation programme (grant agreement No 679681). Dávid Csercsik received funding from the Hungarian National Fund (OTKA NF-104706).

Copyright by the International Federation of Automatic Control (IFAC)

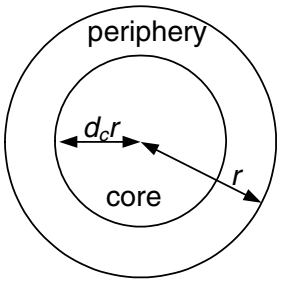

Fig. 1. The definition of the core and periphery of the tumor by the parameter d_c

These assumptions correspond with the latest medical research results by Döme et al. (2007).

2.2 Geometrical considerations

Let us denote the tumor radius with r $[mm]$. We divide the tumor into two parts. By definition, cells closer to the tumor center than $d_c r$ belong to the core, otherwise they belong to the periphery ($d_c \in [0, 1]$ in general) as depicted in Fig 1.

As the diffusion distance is about 150 μm, (Redline and Berger (2014)) we may assume that tumor cells closer to the surface than 150 μm belong to the periphery, and the rest belong to the core. We wish to describe the tumor growth when $r > 0.1$ mm radius. If $r < 0.15$ mm, the whole volume should be considered as periphery. This implies that the function describing the ratio of the core and total radii as a function of r will be 0 for $r < 0.15$ mm, and thus non differentiable at $r = 0.15$ mm. Such functions may be not compatible or may cause inconveniences in model analysis and controller design methods. To overcome this issue, we approximate the exact function with a smooth function as follows:

$$d_c(r) = 1.1 \left(\frac{1}{1 + exp(\frac{0.5-r}{0.333})} \right)^{2.2} - 0.15. \tag{1}$$

The analytic ratio of radii and the smooth approximation are shown is Fig 2. As result, $d_c(r)$ describes how the parameter d_c does depend on the tumor radius r, which will be considered as a state-variable of the model.

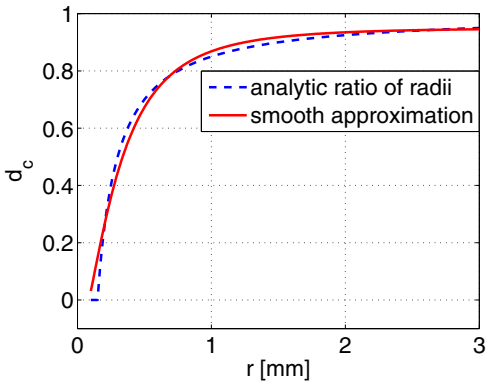

Fig. 2. The approximation of d_c as function of r in order to consider the cells closer to the surface than 150 μm as periphery

2.3 Tumor volume growth

Let us now consider the equations corresponding to volume growth and the effect of growth on the two defined compartments.

The volume of the core (V_C $[mm^3]$) may be calculated as

$$V_C = \frac{4}{3}(d_c r)^3 \pi, \tag{2}$$

while the volume of the periphery (V_P $[mm^3]$) is

$$V_P = \frac{4}{3}(r)^3 \pi - V_C. \tag{3}$$

Let us now assume that the radius of the tumor increases: $r' = r \quad + \Delta r$. In this case the volumes change as follows

$$V_C' = \frac{4}{3}(d_c(r \quad + \Delta r))^3 \pi \tag{4}$$

$$\Delta V_C = V_C' - V_C \tag{5}$$

$$V_P' = \frac{4}{3}(r \quad + \Delta r)^3 \pi - V_C' \tag{6}$$

$$\Delta V_P = V_P' - V_P.$$

We will assume that as the radius of the tumor grows, the core incorporates tumor cells of the periphery (these cells are considered as core cells in the following). This assumption will be formalized and discussed in the state equations (see eq. (10)).

We assume a growth mechanism nonlinearly depending on the cell concentration, originating from the proliferation in the periphery. As a consequence, the g ($[1/\ mm^3]$) growth function is

$$g = \frac{1}{1 + e^{\frac{p_g - [T_p]}{k_g}}}. \tag{7}$$

where $[T_p]$ is the tumor cell concentration in the periphery, and p_g, k_g are parameters. Next, we introduce the mechanisms describing and limiting cell proliferation.

2.4 Proliferation and necrosis

Let us denote the nutrient concentration with $[G]$ ($[1/\ mm^3]$). The value $[G] = 1$ corresponds to the case when the nutrient concentration in the tumor is equal to the nutrient concentration in the healthy tissue in the environment. However, due to the increased vascularization of tumor cells compared to the healthy cells, we assume that the nutrient concentration in tumor cells can be even greater than in healthy cells. If $[G] \geq 1$, it allows normal/supernormal nutrient access for the tumor cells and as a result, fast proliferation will take place without necrosis. If the value of $[G]$ decreases, the proliferation will slow down and necrosis occurs. Finally, if $[G]$ reaches zero, without nutrient acces, the proliferation will stop and only necrosis will take place. The three cases are summarized as follows

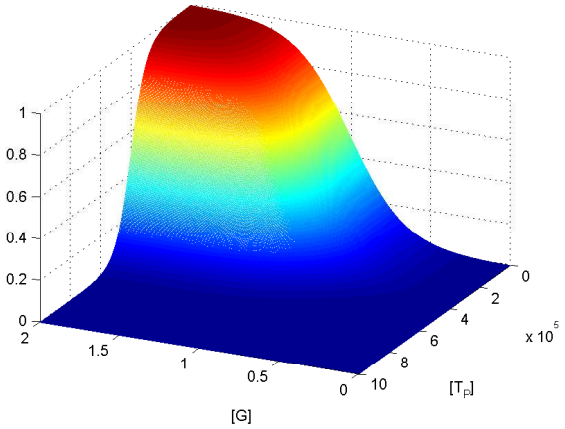

Fig. 3. The proliferation function (f_{prol}) at $p_1 = 1$ $k_1 = 0.17$ $p_2 = 40000$ $k_2 = -5000$ (the constants are determined by the normal range of nutrient and cell concantrations).

$$[G]\begin{cases}[G] \geq 1 & \text{normal/supernormal nutrient access} \rightarrow \\ & \text{fast proliferation rate, no necrosis} \\ 0 < [G] < 1 & \text{decreased nutrient access} \rightarrow \\ & \text{slowed proliferation rate, necrosis starts} \\ [G] = 0 & \text{no nutrient access} \rightarrow \\ & \text{stopped proliferation, maximal necrosis}\end{cases}$$

The nutrient concentration in the core is $[G_C]$, and we assume that the nutrient concentration in the periphery ($[G_P]$) is equal to $([G_C]+1)/2$ (normally, nutrient concentration in the periphery is greater than in the core).

We assume that proliferation takes place only in the periphery (Enderling et al., 2010). Moreover, we assume that the function describing proliferation is saturating with increasing nutrient concentration. The proliferation function (f_{prol}, [1/ mm^3]) describes that the proliferation decays with low nutrient values, and high concentration of tumor cells

$$f_{prol} = \frac{1}{1+e^{\frac{p_1-[G_P]}{k_1}}}\frac{1}{1+e^{\frac{p_2-[T_P]}{k_2}}}, \tag{8}$$

where $[T_P]$ ([1/ mm^3]) denotes the concentration of tumor cells in the periphery. The proliferation function is depicted in Fig. 3.

The consideration of saturation in the case of high tumor cell concentrations originates on the one hand from the assumption that the tumor cells do have a minimal volume, and on the other hand from the consideration that cells in high concentration deplete the nutrients available in the environment. As later (see section 4) we wish to model nutrient availability in more detail, this simple phenomenological approach will be probably refined.

For the aim of simplicity, let us assume that necrotization depends only on $[G_C]$. In this case, the necrotization function (f_{necr}, [1/ mm^3]) takes the following form

$$f_{necr} = \left(\frac{1}{1+e^{\frac{p_3-[G_C]}{k_3}}}\right)^{b_3} \tag{9}$$

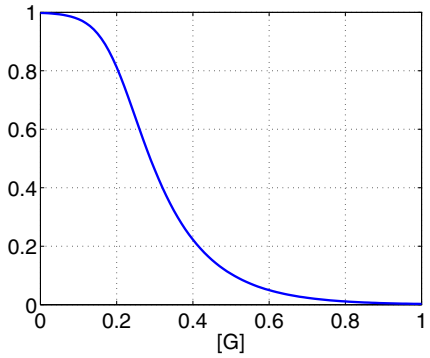

Fig. 4. The necrotization function (f_{necr}) if $p_3 = 0.2$ $k_3 = -0.04$ $b_3 = 0.3$.

The necrotization function is depicted in Fig. 4.

2.5 State space equations

The state equations of the model are as follows

$$\begin{aligned}\frac{dr}{dt} &= a_1 g([T_P]) \\ \frac{dT_C}{dt} &= \frac{dV_C}{V_P}T_P - a_2 f_{necr}([G_C])T_C \\ \frac{dT_P}{dt} &= -\frac{dV_C}{V_P}T_P + a_3 f_{prol}([G_P],[T_P])T_P \\ \frac{dT_{NC}}{dt} &= a_2 f_{necr}([G_C])T_C\end{aligned} \tag{10}$$

T_C and T_P denote the number of tumor cells in the core and in the periphery respectively. T_{NC} denotes the number of necrotic tumor cells in the core. The first terms in the state equations of T_C and T_P describe that as the tumor grows, the core incorporates some cells from the periphery. In the model we assume that the cells of the periphery are homogenously distributed in the total volume. In this case the increase in the core volume dV_C describes how much volume is added from the periphery to the core. dV_C is the infinitesimal limes of ΔV_C, which can be obtained from (5) by substituting Δr with dr. The ratio $\frac{dV_C}{V_P}$ gives the proportion of periphery cells (T_P) which are considered as core cells in the following.

3. SIMULATION RESULTS

Although identification and parameter estimation issues are out of the scope of this article, it has to be noted that parameters have been set to approximately reproduce the data used in (Sápi et al., 2015b). Simulations were carried out using the parameter set in Table 1.

parameter	value	parameter	value
p_g	$4 \cdot 10^5$	k_g	50 000
a_1	0.4	p_2	$4 \cdot 10^5$
a_2	1	k_2	-50 000
a_3	1.6	p_3	0.2
p_1	1	k_3	-0.04
k_1	0.17		

Table 1. Parameter values of the simulations (the dimension of the a_i parameters is mm^3, the other parameters are dimensionless).

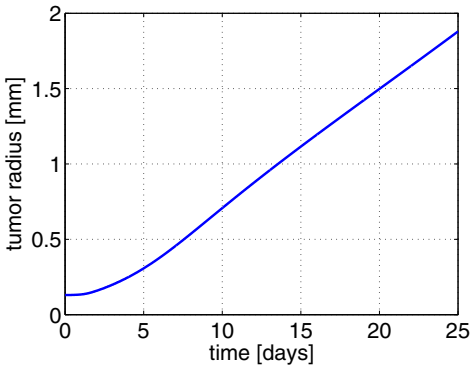

(a) The radius of the tumor (mm)

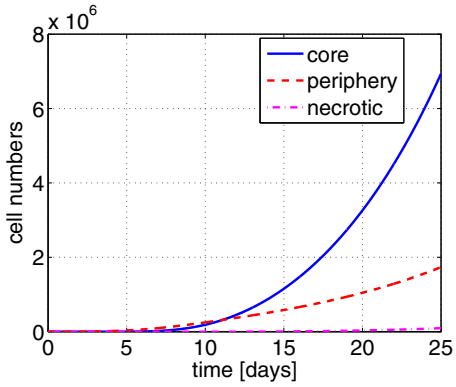

(b) The cell numbers of the tumor

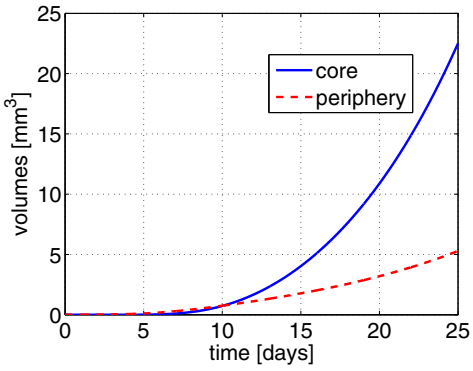

(c) The volumes of the tumor (mm^3)

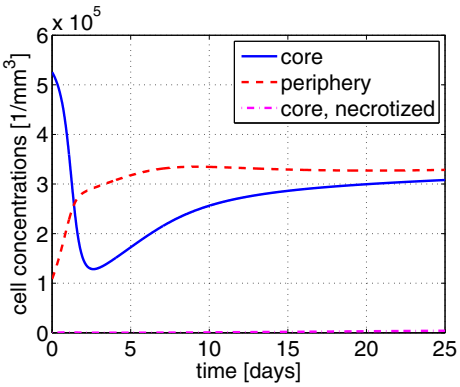

(d) The concentration of the tumor cells ($1/mm^3$)

Fig. 5. Simulation results of tumor radius, cell numbers, tumor volumes and tumor cell concentrations in the case of normal nutrient access

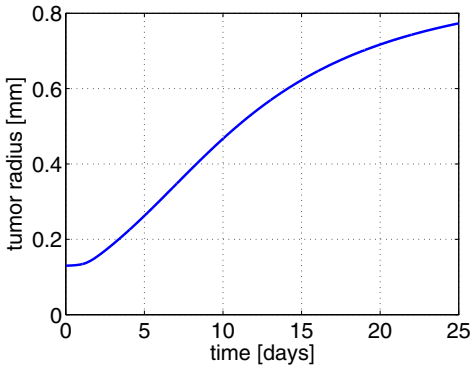

(a) The radius of the tumor (mm)

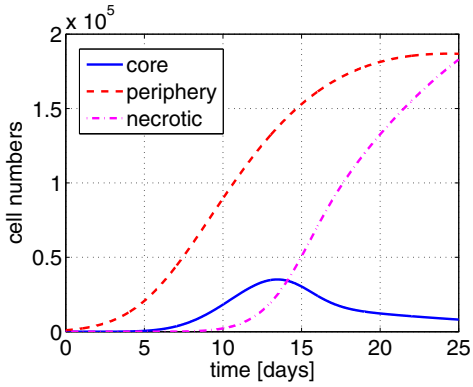

(b) The cell numbers of the tumor

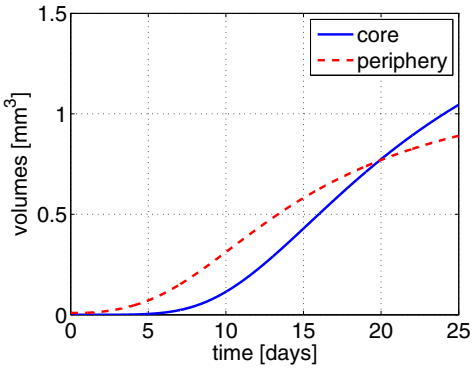

(c) The volumes of the tumor (mm^3)

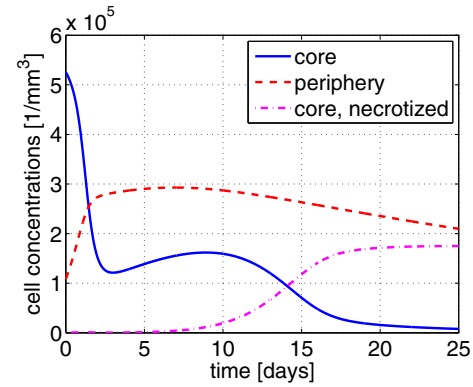

(d) The concentration of the tumor cells ($1/mm^3$)

Fig. 6. Simulation results of tumor radius, cell numbers, tumor volumes and tumor cell concentrations in the case of decreased nutrient access

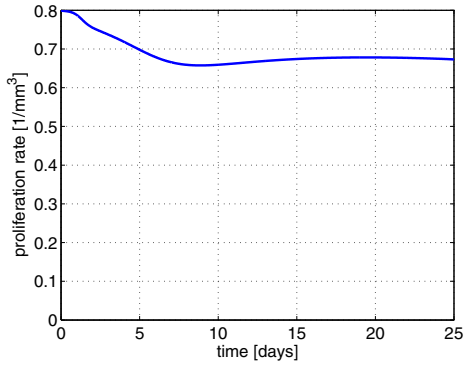

Fig. 7. Simulation result of proliferation rate in the case of normal nutrient access

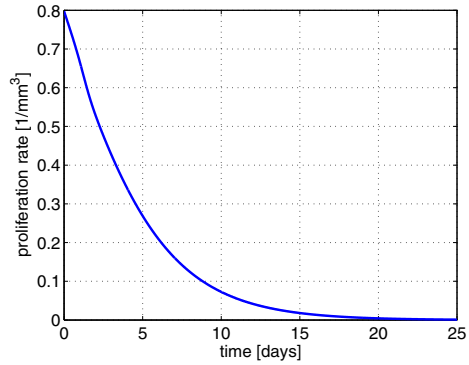

Fig. 8. Simulation result of proliferation rate in the case of decreased nutrient access

3.1 Normal nutrient access

In this case we assume that the nutrient concentration in the tumor (core and periphery) is constantly the same as in the environment ($[G_C] = [G_P] = 1$) during the whole simulation. In real biological conditions, the maximum tumor radius which can be achieved without angiogenesis having normal nutrient access is tipically 1-2 mm, however it depends on the tumor type.

Figs 5a-5d show the simulation results of tumor radius, cell numbers, tumor volumes and tumor cell concentrations in the case of normal nutrient access. The radius of the tumor grows approximately linearly with time because there is no limit for the growth (Fig 5a). The number of the core cells increase faster than the number of periphery cells since the core incorporates tumor cells of the periphery. Due to the fact that normal nutrient access enables fast proliferation, practically there is no necrosis (Fig 5b). As a result, volume curves show similar characteristics as cell number changes, viz. typical exponential growth (Fig 5c). In the beginning of the simulation, the core has small volume with relatively high number of cells, thus the concentration of the core is high. In the periphery, cells are homogenously distributed in a relatively high volume, thus the concentration of the periphery is lower than the concentration of the core. The cell numbers and volumes determine the cell concentrations in the core and in the periphery (Fig 5d).

Fig 7 show the simulation result of proliferation rate in the case of normal nutrient access. The proliferation rate depends on $[G_P]$ and $[T_P]$ (see (8)). Since our assumption was $[G_P] = 1$ during the whole simulation, in this case the proliferation rate depends only on $[T_P]$. From Fig 5d, it is clear that the concentration of the periphery grows, thus the proliferation rate decays. As the growth of periphery concentration slows down, the decline of proliferation rate slows down as well.

3.2 Decreased nutrient access

As the tumor cells are characterized by significantly more intense metabolism, the nutrient concentration in the tumor (mostly in the tumor core) may fall as the pathogenic processes evolve. In the simulations, we defined the nutrient concentration of the core to be equal to an external parameter and in this manner, we analyzed the model dynamics. The external parameter describing nutrient concentration ($[G_C]$) decreases linearly with time as $\frac{d[G_C]}{dt} = -0.05$ and the initial value is equal to the concentration of healthy tissue in the environment $[G_C](0) = 1$.

Tumor radius, cell numbers, tumor volumes and tumor cell concentrations in the case of decreased nutrient access are depicted in Figs 6a-6d. First, as we may see by the comparison of Fig. 5a and Fig. 6a, the final size of the tumor radius is significantly smaller in the case of decreased nutrient; moreover, the curve has a plateau-like characteristic, namely the process shows saturation. Second, as depicted in Fig 6b, due to the lack or nutrients, necrosis is initiated in the tumor core, and necrotic cells appear. In the beginning of the simulation, the number of periphery cells grow fast, while the necrotic curve has a time-delay and starts to grow approximately in the 10th day. Later on, the periphery curve slows down and has a saturation, meanwhile the necrotic curve shows a fast grow. In the end of the simulation, periphery and necrotic cell numbers reach the same value. The number of living core cells starts to grow approximately in the 5th day and due to the fact the core incorporates tumor cells of the periphery, living core cell number continuously increases until the necrotic process become dominant (approximately in the middle of the simulation). After that, the number of living core cells eases down. The tumor volume growth is much more slower than in the case of normal nutrient access (Fig 6c), and both core and periphery curves show saturation. Finally, in the beginning of the simulation, the concentrations of core and periphery show similar characteristics to the normal nutrient case (Fig 6d). However, late on, as necrosis starts, the concentration of living core cells decreases to about zero. The concentration of periphery cells decreases, while the concentration of necrotic core cells increases, and finally they reach a similar steady-state value. It is important to note that if nutrient access is normal, living core and periphery cells have similar concentrations in steady state; while in the lack of nutrient, necrotic core and periphery cells have nearly the same concentrations in steady-state.

Fig 8 shows the simulation result of proliferation rate in the case of decreased nutrient access. Since the nutrient concentration decreases linearly with time, while in the beginning of the simulation the concentration of the pe-

riphery grows, it results in fast reduction of the proliferation rate. When the concentration of the periphery starts to decrease (approximately in the 10th day, see Fig 6d), the slope of decrease of proliferation eases down.

4. DISCUSSION

We proposed a novel tumor growth model, which has the capability to take the proliferation-related processes in the tumor core and in the periphery differently into account, thus is capable of describing spatial aspects of tumor growth on a minimal, two-compartment level. The model qualitatively behaves like expected - based on pathological knowledge - and the growth assuming normal nutrient acces in in good agreement with experimental results Sápi et al. (2015b).

On the one hand the next step is the validation and parameter identification of the model-based on real data.

Furthermore, as we wish to use the model in control and optimization tasks corresponding to anti-angiogenic therapy (d'Onofrio and Gandolfi, 2004; Gevertz, 2011), the model has to be further developed and extended with state variables and mechanisms describing angiogenesis and processes describing the changing blood support of the tumor. Formally, this will mean the inclusion of equations and mechanisms affecting $[G_C]$ which now has been taken into account as an input parameter. Several approaches of modelling angiogenic processes have been published (see eg. Bauer et al. (2007); Arakelyan et al. (2002); Chaplain et al. (2006); Jiang et al. (2005)), however fitting these formalisms in control theoretic framework poses a significant challenge.

When the model will be completed with equations corresponding to angiogenic mechanisms, the next level of the modelling procedure will be the identifiability analysis (Bellu et al., 2007; Saccomani et al., 2003; Walter and Pronzato, 1996; Ljung and Glad, 1994), and the experiment design (Banga and Balsa-Canto, 2008) in order to determine model parameters and their variability in the particular application cases, and make high-fidelity controller design possible.

ACKNOWLEDGEMENTS

The authors would like to thank the help of Paku Sándor from the 1st Department of Pathology and Experimental Cancer Research of the Semmelweis University, Budapest.

REFERENCES

Arakelyan, L., Vainstein, V., and Agur, Z. (2002). A computer algorithm describing the process of vessel formation and maturation, and its use for predicting the effects of anti-angiogenic and anti-maturation therapy on vascular tumor growth. *Angiogenesis*, 5(3), 203–214.

Banga, J.R. and Balsa-Canto, E. (2008). Parameter estimation and optimal experimental design. *Essays Biochem*, 45, 195–209.

Bauer, A.L., Jackson, T.L., and Jiang, Y. (2007). A cell-based model exhibiting branching and anastomosis during tumor-induced angiogenesis. *Biophysical journal*, 92(9), 3105–3121.

Bellu, G., Saccomani, M., Audoly, S., and D'Angio, L. (2007). DAISY: A new software tool to test global identifiability of biological and physiological systems. *Comput Methods Programs Biomed*, 88, 52–61.

Byrne, H.M., King, J.R., McElwain, D.S., and Preziosi, L. (2003). A two-phase model of solid tumour growth. *Applied Mathematics Letters*, 16(4), 567–573.

Chaplain, M.A., McDougall, S.R., and Anderson, A. (2006). Mathematical modeling of tumor-induced angiogenesis. *Annu. Rev. Biomed. Eng.*, 8, 233–257.

Döme, B., Hendrix, M., Paku, S., Tóvári, J., and Tímár, J. (2007). Alternative vascularization mechanisms in cancer: Pathology and therapeutic implications. *Am J Pathol*, 170(1), 1–15.

d'Onofrio, A. and Gandolfi, A. (2004). Tumour eradication by antiangiogenic therapy: analysis and extensions of the model by hahnfeldt et al.(1999). *Mathematical Biosciences*, 191(2), 159–184.

Enderling, H., Hlatky, L., and Hahnfeldt, P. (2010). Tumor morphological evolution: directed migration and gain and loss of the self-metastatic phenotype. *Biology direct*, 5(1), 1.

Femke, H. and Griffioen, A. (2007). Tumour vascularization: sprouting angiogenesis and beyond. *Cancer Metastasis Rev*, 26(3–4), 489–502.

Gevertz, J.L. (2011). Computational modeling of tumor response to vascular-targeting therapiespart i: validation. *Computational and mathematical methods in medicine*, 2011.

Gunawardena, J. (2003). Chemical reaction network theory for in-silico biologists. URL `http://vcp.med.harvard.edu/papers/crnt.pdf`.

Hahnfeldt, P., Panigrahy, D., Folkman, J., and Hlatky, L. (1999). Tumor development under angiogenic signaling a dynamical theory of tumor growth, treatment response, and postvascular dormancy. *Cancer research*, 59(19), 4770–4775.

Jiang, Y., Pjesivac-Grbovic, J., Cantrell, C., and Freyer, J.P. (2005). A multiscale model for avascular tumor growth. *Biophysical journal*, 89(6), 3884–3894.

Ljung, L. and Glad, T. (1994). On global identifiability of arbitrary model parametrizations. *Automatica*, 30, 265–276.

Redline, S. and Berger, N. (2014). *Impact of Sleep and Sleep Disturbances on Obesity and Cancer*. Springer-Verlag New York.

Saccomani, M.P., Audoly, S., and D'Angio, L. (2003). Parameter identifiability of nonlinear systems: the role of initial conditions. *Automatica*, 39, 619–632.

Sápi, J., Drexler, D.A., and Kovács, L. (2015a). Comparison of mathematical tumor growth models. In *2015 IEEE 13th International Symposium on Intelligent Systems and Informatics (SISY)*, 323–328.

Sápi, J., Kovács, L., Drexler, D.A., Kocsis, P., Gajári, D., and Sápi, Z. (2015b). Tumor volume estimation and quasi-continuous administration for most effective bevacizumab therapy. *PloS ONE*, 10(11), e0142190.

Walter, E. and Pronzato, L. (1996). On the identifiability and distinguishability of nonlinear parametric models. *Math Comput Simul*, 42, 124–134.

Yang, H.M. (2012). Mathematical modeling of solid cancer growth with angiogenesis. *Theoretical Biology and Medical Modelling*, 9(1), 1.